JOURNAL OF GEOPHYSICAL RESEARCH, VOL. 111, D24103, doi:10.1029/2005JD006939, 2006

Sensitivity of global tropospheric ozone and fine particulate matter concentrations to climate change

Pavan Nandan Racherla[1] and Peter J. Adams[2]

Received 1 December 2005; revised 3 July 2006; accepted 10 August 2006; published 16 December 2006.

[1] An integrated global model of climate, tropospheric gas phase chemistry, and aerosols has been used to investigate the sensitivity of global ozone and fine particulate matter concentrations to climate change. Two simulations corresponding to present (1990s) and future (2050s) climates have been performed and compared. A future climate has been imposed using ocean boundary conditions corresponding to the Intergovernmental Panel on Climate Change SRES A2 scenario for the 2050s decade, resulting in an increase in the global annual average values of the surface air temperature by 1.7°C, the lower tropospheric specific humidity by 0.9 g H_2O/kg air, and the precipitation by 0.15 mm d^{-1}. Present-day anthropogenic emissions have been used in both simulations while climate-sensitive natural emissions were allowed to vary with the simulated climate. The tropospheric ozone burden in the future climate run decreased by 5%, and its lifetime decreased from 27.8 to 25.3 days. The tropospheric ozone change is driven primarily by increased ozone loss rates through ozone photolysis in the presence of water vapor, which on a global scale, more than compensate for the increased ozone chemical production associated with increased temperatures. At the model surface layer, over remote regions, ozone mixing ratios decreased by 1–3 ppbv, while polluted regions showed a relatively smaller decrease of 0–1 ppbv and increased by 1–5 ppbv in some cases. The global burdens and lifetimes of fine particulate matter species in the future climate run decreased by 2 to 18% because of increased wet deposition loss rates associated with increased precipitation. At the model surface layer, there are regions of decreases and increases in the concentrations of fine particulate matter species. The increased surface layer concentrations of some fine particulate matter species is primarily driven by lower regional-scale precipitation and increased secondary production, where applicable. The robustness of the predicted regional-scale changes for fine particulate matter species is strongly dependent upon the predicted regional-scale precipitation changes.

Citation: Racherla, P. N., and P. J. Adams (2006), Sensitivity of global tropospheric ozone and fine particulate matter concentrations to climate change, *J. Geophys. Res.*, *111*, D24103, doi:10.1029/2005JD006939.

1. Introduction

[2] Several studies have suggested links between ozone and fine particulate matter (PM) concentrations and mortality rates in addition to numerous other health problems [*Schwartz*, 1996; *Dockery et al.*, 1993; *Krewski et al.*, 2003]. Hence reduction of ozone and fine PM (PM_f) concentrations has become one of the key objectives of air quality policy and regulation for many governments. Both ozone and PM_f concentrations are linked sensitively to weather and climate. Key meteorological parameters influencing pollutant concentrations include temperature, sunlight, cloudiness, wind speeds and precipitation. Changes in any or all of these meteorological parameters due to climate change will necessarily impact concentrations of ozone and PM_f. However, the direction of change itself is often unclear because of multiple competing effects.

[3] The motivation for this work is twofold. First, climate change impacts on air quality may affect long-term air quality planning. Currently, air quality planning on a short term accounts for changes in emissions but assumes unchanged climate. On longer timescales, it may be necessary to loosen this assumption. While many air quality decisions need only be made on short timescales, future investments in the energy infrastructure and power plant regulations have long-term implications where it may be useful to consider their impacts under changed climate scenarios. Second, the impacts of climate change on many important issues have been considered to assess the overall danger [*Intergovernmental Panel on Climate Change* (*IPCC*), 2001]. However, the impacts of climate change on air quality are not very well understood. A better understanding

[1]Department of Engineering and Public Policy and Department of Mechanical Engineering, Carnegie Mellon University, Pittsburgh, Pennsylvania, USA.
[2]Department of Civil and Environmental Engineering and Department of Engineering and Public Policy, Carnegie Mellon University, Pittsburgh, Pennsylvania, USA.

0148-0227/06/2005JD006939$09.00

of the impacts of climate change on air quality will contribute to a more holistic assessment of climate change impacts.

[4] Some previous studies have assessed the impact of different meteorological parameters on air pollution at regional and global scales. *Sillman and Samson* [1995] performed regional-scale and 1-D global-scale simulations to study the impact of temperature on ozone concentrations. They concluded that ozone increases with temperature in urban and polluted rural environments, with the increase driven largely by peroxyacetyl nitrate (PAN) chemistry. On the other hand, their 1-D global-scale simulations suggest that increased temperature in the polluted boundary layer may not lead to increased ozone in the free troposphere because increased export of ozone is countered by decreased export of NO_x. *Aw and Kleeman* [2003] used an urban-scale air quality model to study the effect of interannual temperature variability on air pollution in the Southern California region. Their results indicate that ozone and nonvolatile secondary PM generally increase at higher temperatures due to increased gas phase reaction rates, while semivolatile secondary PM could increase or decrease depending on the ambient conditions. In an urban-scale model study of the Milan region, *Baertsch-Ritter et al.* [2004] studied the effects of various meteorological conditions such as temperature, wind speeds and mixing height on ozone concentrations. As a base case they modeled an ozone episode that occurred on 13 May 1998 at 15h CET, and compared it with model simulations for the same period that incorporated the variation of individual meteorological parameters. They found that increased temperature increased peak O_3 by 10 ppb $^{\circ}C^{-1}$ and the domain-average O_3 concentrations by 2.8 ppb $^{\circ}C^{-1}$. With regards to increasing wind speeds, their results suggest an increase in VOC (volatile organic compounds) limited areas, because the VOC-limited ozone chemistry induced by point sources is spread over a larger area.

[5] *Stevenson et al.* [2000] and *Johnson et al.* [2001] studied the impact of climate change on tropospheric ozone radiative forcing and methane lifetime using a 3-D chemical transport model (CTM). Their climate change simulations indicate that the dominant change in the tropospheric ozone budget resulting from climate change is an increased destruction of ozone due to increased absolute humidity. *Liao et al.* [2006], in a separate study with the same model [*Liao et al.*, 2003, 2004] as used in our study, found that the year 2100 global ozone and aerosol burdens due to CO_2-driven climate change alone are lower than the present-day levels, as a result of faster ozone removal and increased aerosol wet deposition, respectively.

[6] Previous studies, although relevant, have certain limitations. Regional-scale modeling studies have focused on perturbations of a small set of individual meteorological variables such as temperature and their effect on air pollution. This is a potentially serious limitation because changes in meteorological variables such as temperature, relative humidity, mixing height and wind speeds seldom occur in isolation and each affects ozone and PM_f concentrations. Another limitation of regional-scale studies is that their assumption of constant boundary conditions (BCs) neglects climate change impacts outside their domain. Furthermore, regional-scale modeling studies are limited to specific geographical locations.

[7] Previous global-scale modeling studies have examined the impact of climate change on ozone and its precursors. Only one previous study [*Liao et al.*, 2006] (hereafter referred to as LIP06) addressed the simultaneous impact of climate change on PM_f concentrations. In contrast to LIP06, which focused on the impact of climate change on direct radiative forcings by ozone and PM_f, the current study is motivated by the impacts of climate change on air quality. By way of methodology, LIP06 employed a version of the model used in the current study that uses a q flux ocean [*Hansen et al.*, 1983], where the sea surface temperatures (SSTs) and ocean ice respond to climate change. In contrast, the current study employs a version that uses prescribed SSTs and ocean ice. Finally, LIP06 predicts atmospheric ozone and PM_f concentrations for the year 2100. The current study is potentially more useful for near-term policy making given projections to 2050. Also, to address air quality concerns, we present here regional-scale budgets and changes as well as global-scale ones.

[8] In this study we employ a global model of climate, tropospheric gas phase chemistry and aerosols [*Liao et al.*, 2003, 2004] to study the sensitivity of both global ozone and PM_f concentrations to climate change. Details of the model and simulation methods are provided in section 2. Ozone and PM_f results are discussed in section 3. Finally, the conclusions are presented in section 4.

2. Methods

2.1. Model Description

2.1.1. Overview

[9] We utilize in this work a "unified" model [*Liao et al.*, 2003, 2004], which consists of three major components: (1) the Goddard Institute for Space Studies general circulation model II′ (GISS GCM II′) [*Hansen et al.*, 1983; *Rind and Lerner*, 1996; *Rind et al.*, 1999]; (2) the Harvard tropospheric O_3-NO_x-hydrocarbon chemical model [*Mickley et al.*, 1999]; and (3) an aerosol model [*Adams et al.*, 1999; *Chung and Seinfeld*, 2002; *Liao et al.*, 2003, 2004].

[10] The GISS GCM II′ has a horizontal resolution of 4° latitude by 5° longitude, with nine vertical layers centered at 959, 894, 786, 634, 468, 321, 201, 103, and 26 hPa. The GCM's troposphere extends from approximately 984 hPa to 150 hPa. The version of GISS GCM II′ incorporated in the current study uses specified monthly mean ocean boundary conditions (OBCs) in the form of SSTs, sea ice coverage and sea ice mass. The dynamical time step of the GCM is 1 hour. Necessary GCM variables are passed to the tropospheric chemistry and aerosol modules every 4 hours.

[11] A total of 88 gas and aerosol phase species are transported in the "unified" model. Of these, 24 species are used to describe O_3-NO_x-hydrocarbon chemistry; the remainder are for simulation of sulfate, nitrate, ammonium, black carbon (BC), primary organic aerosol (POA), secondary organic aerosol (SOA), dust, and sea salt. As described by *Chung and Seinfeld* [2002], reactive terpenes that, upon atmospheric oxidation, lead to semivolatile products that form SOA, are grouped into five hydrocarbon categories according to the values of their experimentally measured aerosol yield parameters. SOA formation due to the oxida-

tion by O_3 and OH is considered together, and it is simulated using a two-product model. On the other hand, SOA formation due to the oxidation by NO_3 is simulated using a one-product model. Sea salt is represented using 11 size bins, with 5 size bins having dry radius ≤ 1 μm, while dust is represented using 6 size bins, with 2 size bins having dry radius ≤ 1 μm [*Liao et al.*, 2004]. The mass in each size bin is treated as a separate species with its own deposition behavior, but intersectional mass transfer by aerosol microphysics is not simulated.

[12] The model is constrained in the stratosphere by applying flux upper boundary conditions between the seventh and eighth model layers (approximately 150 hPa) to represent transport across the tropopause [*Wang et al.*, 1998]. As described by *Mickley et al.* [1999], the flux upper boundary conditions for ozone is based on the observed latitudinally and seasonally dependent cross-tropopause air mass fluxes [*Appenzeller et al.*, 1996], along with ozonesonde measurements at 100 hPa [*Logan*, 1999]. In the current study, we specify a stratospheric ozone flux of 400 Tg yr^{-1}, a value that was used in the previous model versions [*Liao et al.*, 2003]. We use this value for both the present and future simulations discussed in section 2.2. By doing so, this study does not investigate the influence of increased stratospheric ozone flux under climate change, which is likely to increase tropospheric ozone [*Collins et al.*, 2003].

[13] As described by *Wang et al.* [1998], the dry deposition of all gas phase species is determined based on the resistance-in-series scheme of *Wesely* [1989], wherein the dry deposition velocity is inversely proportional to the sum of the aerodynamic, quasi-laminar sublayer and surface resistances. The aerodynamic and quasi-laminar sublayer resistances are calculated based on the GCM surface fluxes of momentum and heat while the surface resistance is a function of the surface type and the species. Particle dry deposition velocities of all nondust, non-sea-salt species are calculated based on the treatment for sulfate described by *Koch et al.* [1999] while those for dust, sea salt, and associated species are based on the work of *Liao et al.* [2004]. Wet deposition is coupled with the GCM treatment of clouds and precipitation [*Koch et al.*, 1999; *Del Genio and Yao*, 1993; *Del Genio et al.*, 1996]. The size-dependent wet deposition treatment for dust and sea salt is described by *Liao et al.* [2004] and the references therein.

[14] Anthropogenic and natural emissions used in the model are summarized in *Liao et al.* [2003, 2004]. Climate-sensitive emissions include isoprene [*Guenther et al.*, 1995; *Wang et al.*, 1998], lightning and soil NO_x [*Wang et al.*, 1998], DMS [*Kettle et al.*, 1999], sea salt and mineral dust [*Liao et al.*, 2004]. The meteorological variables that influence these emissions include temperature (isoprene, soil NO_x and DMS), solar radiation (isoprene), precipitation (soil NO_x and mineral dust), surface wind speed (DMS, sea salt and mineral dust) and frequency of convective events (lightning NO_x). Therefore the model treats the climate sensitivity of these emissions such that the emissions rates of these species change between the present and future simulations discussed in section 2.2. The climate sensitivity of monoterpenes and sesquiterpenes emissions, which is important to the formation of SOA, is not considered in this study.

2.1.2. Heterogeneous Chemistry

[15] The only significant change compared to previous versions of the model is with regards to heterogeneous chemistry. Important heterogeneous reactions considered in the "unified" model include hydrolysis of N_2O_5 on wetted aerosol surfaces of sulfate, nitrate, ammonium, OC, and sea salt; dust uptake of SO_2, HNO_3, and O_3; and sea salt uptake of SO_2. SO_2 and HNO_3 deposited on dust particles are assumed to oxidize to SO_4^{2-} and NO_3^-, respectively. The SO_4^{2-} and NO_3^- formed on dust are treated as separate species from other forms of sulfate and nitrate, and we refer to them as SO_4^{2-}(D) and NO_3^-(D). The fraction of SO_2 that is taken up by sea salt and oxidized by H_2O_2 and O_3 (in aqueous sea salt aerosols) to sulfate is also tracked as a separate species denoted SO_4^{2-}(SSO). Sulfate and nitrate not associated with sea salt or dust are simply designated as SO_4^{2-} and NO_3^-, respectively.

[16] *Liao et al.* [2004] deliberately used high estimates of uptake coefficients to bound the impacts of heterogeneous reactions on gas phase chemistry and aerosol formation. In this study, we used best guess uptake coefficients related to the heterogeneous reactions. The major change is with the uptake coefficient for N_2O_5 hydrolysis, which now depends on aerosol type, relative humidity, and temperature [*Kane et al.*, 2001; *Thornton et al.*, 2003; *Hallquist et al.*, 2003], in contrast with the single uptake coefficient of 0.1 used for all aerosol types by *Liao et al.* [2004]. These new coefficients lead to less hydrolysis of N_2O_5. The new dust uptake coefficients for ozone and HNO_3 are 10^{-5} [*Bauer and Koch*, 2005] and 1.1×10^{-3} [*Bian and Zender*, 2003], respectively, in contrast with the values of 5×10^{-5} and 0.1 used by *Liao et al.* [2004].

2.1.3. Fine PM Definition

[17] In the absence of size-resolved treatment of SO_4^{2-}, NO_3^-, NH_4^+, BC, POA and SOA in the "unified" model, we assume that these species reside in particles associated with the accumulation mode. Hereafter, we refer to these species as fine PM. For dust and sea salt, we choose to show the total amount. For SO_4^{2-}(D), NO_3^-(D) and SO_4^{2-}(SSO), we do not include them in fine PM for simplicity and because they globally account for less than 10% of their burdens.

2.2. Simulations

[18] Two runs, each of five and a half year duration, were performed with the first six months ignored to allow for model initialization. All results, annual, seasonal or monthly refer to averages over the remaining five years. The first run corresponds to present-day (1990s) climate while the second run corresponds to a future (2050s) climate scenario. Hereafter, we refer to these runs as present and future runs, and abbreviate them as PR and FR, respectively. Present day anthropogenic emissions were used in both the runs while climate-sensitive natural emissions were allowed to vary with the simulated climate (see section 2.1.1).

[19] A present-day CO_2 mixing ratio of 370 ppmv was specified in both the runs. Future climate is imposed by changing the OBCs that drive the general circulation model. Changing the OBCs is an alternative method for imposing climate change that is attractive because of the large amounts of computer time that would be required for simulating the equilibriaton of the ocean, if a greenhouse gas forcing were imposed on the system [*Cess et al.*, 1990].

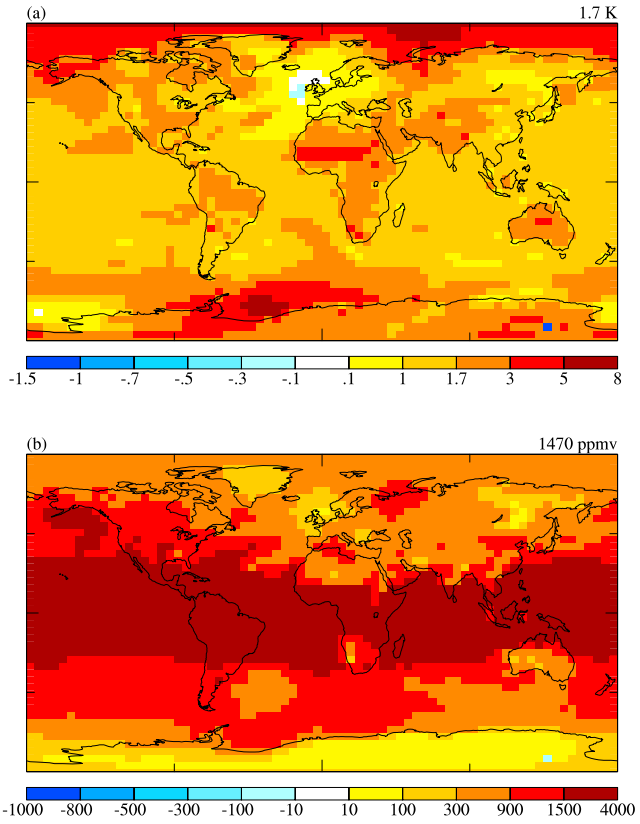

Figure 1. Surface layer (984–934 hPa) annual average differences (future run (FR) minus present run (PR)) of (a) air temperatures and (b) water vapor mixing ratios. The global annual average differences and units are indicated above the top right corner.

The OBCs used in this study were obtained from a transient simulation performed using a fully coupled atmosphere-ocean GCM (the GISS Model III [*Russell et al.*, 1995; R. Healy, personal communication, 2005]). That model was run 250 years total, starting in 1850. Simulations based on the trends in the concentrations of atmospheric greenhouse gases prescribed by the IPCC SRES A2 scenario [*Robertson et al.*, 2001] and sulfate/carbonaceous aerosols described by *Koch* [2001] were started in 1990, thus allowing for a spin-up period of 140 years. The model was initialized from the National Meteorological Center atmospheric observations for 1 December 1977 and *Levitus* [1982] ocean climatological temperature and salinity fields. The present and future OBCs in the current study correspond to a decadal average of the 1990s and 2050s from the above simulation, respectively, with month-to-month variability.

2.3. Predicted Climate Change

[20] It takes approximately three months during the 6-month model initialization period for the surface layer air temperatures to equilibrate to the changed OBCs, resulting in a 1.7°C increase in the annually and globally averaged surface layer air temperature. The spatial distribution of the surface layer air temperature differences between the present and future runs is shown in Figure 1a. The predicted differences shown in Figure 1a closely resemble the mid-21st century surface layer temperature differences for the A2 scenario shown in the IPCCs Third Assessment Report [*IPCC*, 2001].

[21] Changes in the hydrologic cycle play a key role in the ozone and PM_f results, as discussed subsequently. The spatial pattern of the predicted changes in the surface layer water vapor mixing ratios are shown in Figure 1b. This corresponds to an increase of 0.9 g H_2O/kg air (10%) in the annually and globally averaged lower tropospheric specific humidity, and a 1.62 Eg increase (14%) in the global tropospheric water vapor burden. The predicted increase (%) in lower tropospheric (984–854 hPa) specific humidity per degree of global warming is 5.8% $°C^{-1}$, and it is consistent with other GCM simulations [*Soden et al.*, 2005; IPCC, 2001]. The global annual average precipitation increased by 0.15 mm d^{-1} (4.7%) relative to the present run. The predicted precipitation increase (%) per degree of global warming is 2.8% $°C^{-1}$, and it agrees well with the ensemble mean of 3.6% $°C^{-1}$ obtained from 19 AOGCM simulations [*Allen and Ingram*, 2002].

[22] In order to evaluate the statistical significance of the predicted global precipitation increase, a Welch two-sample t test comparing the global annual average precipitation (mm d^{-1}) distributions between the present run (μ = 3.16 and σ = 0.06) and the future run (μ = 3.31 and σ = 0.08) was performed. This test indicates that the predicted 0.15 mm d^{-1} increase in the global annual average precipitation is significant at a 95% confidence level. However, a similar analysis on the predicted changes in the regional-scale precipitation reveals that they are not significant at a 95% confidence level. As a result, model predictions that depend strongly on the predicted regional-scale precipitation changes have a significant uncertainty associated with them.

3. Results

3.1. Ozone

3.1.1. Tropospheric Ozone Budget

[23] The annual tropospheric ozone (O_3^t) budget in the present and future runs is shown in Table 1. The budget presented here is for the odd oxygen (O_x) family defined as the sum of ozone, O, NO_2, 2 × NO_3, 3 × N_2O_5, HNO_4, HNO_3, and the peroxyacylnitrates. By evaluating the budget for the odd oxygen chemical family as defined above, the rapid cycling between the members included is better accounted for. For example, free oxygen atoms are included, as there is rapid cycling between O and O_3. Also, NO_2 is included, as there is rapid cycling between NO_2 and O/O_3. Similarly, other NO_y species are included.

[24] In the future run, the most noticeable changes in the O_3^t budget are the decreased O_3^t lifetime (τ) from 27.8 to 25.3 days, an increased O_3^t chemical production (by 145 Tg yr^{-1} or 4%) and an increased O_3^t destruction rate through $O(^1D) + H_2O$ (by 120 Tg yr^{-1} or 6.8%). The future O_3^t burden itself decreased by 5.6% (17 Tg) relative to the present run. The predicted changes in the O_3^t budget agree well with the simulation of *Stevenson et al.* [2000] for a similar time period (2060) and scenario (IPCC SRES A2). Their O_3^t budget indicates a decrease of 4% in the O_3^t burden along with a 3% increase in the O_3^t chemical production and a 7% increase in the O_3^t destruction through $O(^1D) + H_2O$.

[25] By utilizing the steady state definition of the lifetime of a species (equation (1)) and linearizing the changes in the

Table 1. Annual Global Budget for Tropospheric Odd Oxygen (O_x)[a]

	Present Run	Future Run
Sources, Tg yr^{-1}		
Chemical production		
NO + HO_2	2270	2325
NO + CH_3O_2	820	850
NO + RO_2	520	580
Total	3610	3755
Stratospheric flux	400	400
Total	4010	4155
Sinks, Tg yr^{-1}		
Chemical loss		
$O(^1D)$ + H_2O	1765	1885
O_3 + HO_2	885	890
Other reactions	690	730
Total	3320	3505
Dry deposition	670	650
Total	4010	4155
Net chemical production, Tg yr^{-1}	290	250
Burden, Tg	305	288
Lifetime, days	27.8	25.3

[a]See section 3.1.1 for the definition of O_x.

O_3^t lifetime and the O_3^t sources (S) about the present run, the fractional change in the O_3^t burden (M) can be approximated using equation (2).

$$\tau = \frac{M}{S} \tag{1}$$

$$\frac{\Delta M}{M_{PR}} = \left(\frac{\Delta \tau}{\tau_{PR}}\right)_{S_{PR}} + \left(\frac{\Delta S}{S_{PR}}\right)_{\tau_{PR}} \tag{2}$$

Hereafter, we refer to the first and second terms on the right hand side of equation 2 as the sink effect and the source effect, respectively. Application of equation (2) to the O_3^t budget shows that the source effect (+3.6%) is dominated by the sink effect (−9.0%) on a global scale. However, increased sources (O_3^t chemical production) play an important role on a regional scale, as discussed subsequently. The increased O_3^t chemical production is due to warmer temperatures that result in (1) increased chemical reaction rates and (2) a less stable PAN, causing a greater fraction of the oxidized nitrogen to be present as NO_x [*Sillman and Samson*, 1995].

[26] The shortened O_3^t lifetime is driven primarily by increased O_3^t destruction rates due to the reaction (R2),

(R1) $$O_3 + h\nu \longrightarrow O(^1D) + O_2$$

(R2) $$O(^1D) + H_2O \longrightarrow 2\ OH\cdot$$

which, in turn, is a consequence of increased global water vapor concentrations. Because the burdens in the two runs are different, the impact of increased O_3^t destruction rate by the above reaction is captured better by its contribution to the shortened O_3^t lifetime. Since the O_3^t lifetime with respect to each loss mechanism has decreased relative to the present run, we define a new parameter, $\tau_{\Delta proc}$, to assess their relative contributions to the shortened overall O_3^t lifetime. The $\tau_{\Delta proc}$ with respect to a loss mechanism (l) is what the new overall O_3^t lifetime would be if the O_3^t lifetime with respect to that mechanism alone changed in the future run. The calculation of $\tau_{\Delta proc}$ is illustrated in equation (3):

$$\frac{1}{\tau_{\Delta proc}} = \sum_{j(j\neq l)} \frac{1}{\tau_{PR,j}} + \frac{1}{\tau_{FR,l}} \tag{3}$$

where $\tau_{PR,j}$ is the O_3^t process lifetime with respect to loss mechanism j in the present run and $\tau_{FR,l}$ is the O_3^t process lifetime with respect to loss mechanism l in the future run. O_3^t process lifetimes and $\tau_{\Delta proc}$ values are shown in Table 2. It shows that the reduction in O_3^t lifetime with respect to reaction (R2) (from 63 to 56 days) would, by itself, decrease the overall O_3^t lifetime to 26.2 days, while decreased O_3^t lifetimes with respect to other loss mechanisms further reduce the overall O_3^t lifetime by smaller amounts.

3.1.2. Surface Layer Ozone

[27] Annual average surface layer ozone (O_3^s) mixing ratios in the present run are shown in Figure 2a, while Figure 2b shows the differences (FR - PR) in O_3^s mixing ratios between the two simulations. In the future run, over most remote regions (unpolluted or marine), O_3^s mixing ratios decreased by 1–3 ppbv. On the other hand, regions with high ozone precursor emissions showed a relatively smaller decrease (0–1 ppbv) in O_3^s mixing ratios and an increase in some cases (eastern United States, eastern China, parts of the Indian Subcontinent, the Mediterranean and South Africa).

[28] Over regions where the annual average O_3^s mixing ratios increased in the future run, the seasonal O_3^s budgets indicate that this increase is dominated by summertime increases, which are in the range of 3–9 ppbv. To illustrate this the summer (June/July/August) and winter (December/January/February) O_3^s budgets for the eastern United States (95–80°W, 32–40°N) are presented in Table 3. The sink and source effects for each season shows that the summertime O_3^s increase occurs primarily due to the increased O_3^s chemical production. The relatively longer O_3^s lifetime also plays an important role when compared to the wintertime O_3^s changes, as discussed subsequently. The increased O_3^s chemical production is due to warmer temperatures, which cause the PAN $\leftrightarrow$ NO_x equilibrium to favor NO_x, and increased biogenic HC emissions as suggested by the sensitivity studies of *Liao et al.* [2006]. The longer O_3^s lifetime is due to the reduced O_3^s dry deposition flux, which more than compensates for the faster O_3^s chemical loss rates. The reduced O_3^s dry deposition flux is due to increased aerodynamic and quasi-laminar sublayer resistance. The change in surface resistance itself plays a negligible role

Table 2. Process Lifetimes for Tropospheric Ozone

	Process Lifetime, days		
Loss Mechanism	Present Run	Future Run	$\tau_{\Delta proc}$[a]
$O(^1D)$ + H_2O	63	56	26.2
O_3 + HO_2	126	118	27.4
Other reactions	161	144	27.2
Dry deposition	167	162	27.6

[a]See section 3.1.1 for the definition of $\tau_{\Delta proc}$.

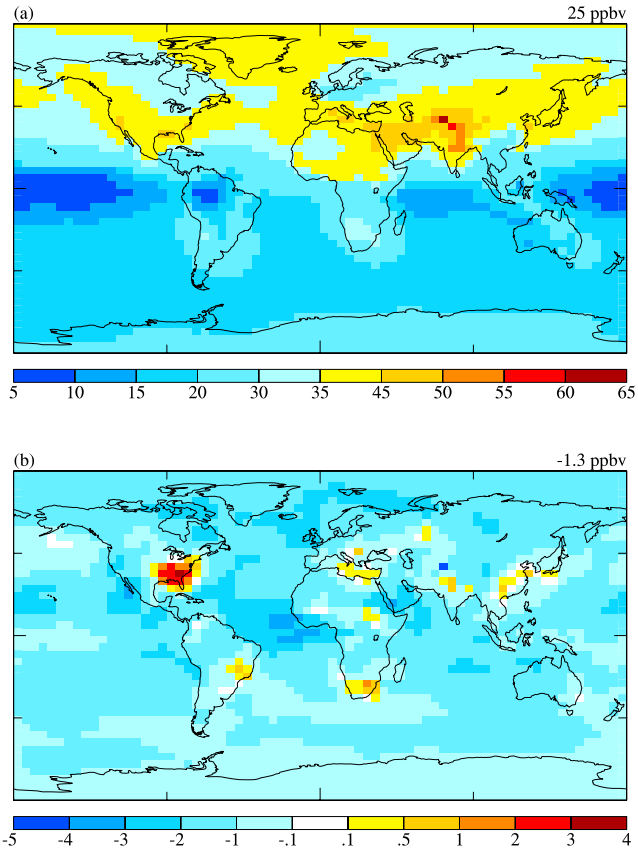

Figure 2. (a) Surface layer (984–934 hPa) annual-average mixing ratios (ppbv) of ozone in the present run and (b) annual average differences (future run (FR) minus present run (PR)) of ozone mixing ratios. The global annual average mixing ratio (or difference) and units are indicated above the top right corner.

because key surface parameters such as the leaf area index are being held constant. Moreover, the summertime surface resistances are small relative to the aerodynamic and quasi-laminar sublayer resistances. In contrast with the summertime O_3^s increases, O_3^s mixing ratios remained nearly unchanged during the winter due to increased O_3^s dry deposition loss rates, which more than compensated for the increased O_3^s chemical production.

[29] The O_3^s changes over the eastern United States indicate that while changes in O_3^s dry deposition played a minor role globally, it plays an important role at the surface layer. This is not surprising considering that dry deposition is the dominant surface layer sink for ozone. The seasonal pattern of the predicted O_3^s changes shows that the increased O_3^s chemical production, by itself, may not be sufficient to cause increased O_3^s mixing ratios. On the other hand, as suggested by the summertime increases, increased O_3^s chemical production could result in increased O_3^s levels if the O_3^s dry deposition removal rates decreased or remain nearly unchanged.

3.2. Fine PM Species

3.2.1. Global Budgets

[30] Annual global budgets for PM_f species in the present and future runs are shown in Table 4. It can be seen from Table 4 that wet deposition is the dominant removal mechanism for SO_4^{2-}, NO_3^-, NH_4^+ and SOA, where it accounts for more than 80% of the removal of these species from the atmosphere. For BC and POA, removal by dry deposition is also important. With regards to a comparison of the budgets between the present and future runs, the reduced future global burdens and lifetimes for all the species is readily noticeable. Again, application of equation (2) helps quantify the relative importance of the sink and source effects to the global burden decrease for each species. This is also shown in Table 4. For the PM_f inorganic species, the sink effect outweighs the source effect. For the PM_f organic species, this is true for BC and POA, as their sources, i.e., primary emissions, are held constant between the two runs. However, for SOA, the source effect in the form of reduced aerosol:gas ratio is the dominant factor in the global burden decrease.

[31] Changes in the hydrologic cycle in the future run play a key role in the shortened lifetimes of the PM_f species. The shortened lifetimes of all the PM_f species is due to increased wet deposition rates, which, in turn, is a result of the increased annual average global precipitation from 3.15 mm d^{-1} to 3.3 mm d^{-1} predicted by the GCM. While precipitation effects dominate the response of other species, the reduced SOA burden in the future run is primarily driven by reduced partitioning of gas phase secondary organics (SO) into the aerosol phase, as a result of warmer temperatures. Increased precipitation itself plays a relatively minor role by reducing the total secondary organic levels from 1.74 to 1.73 Tg.

3.2.2. Surface Layer PM_f

[32] Annual average surface layer concentrations of PM_f species in the present run are shown in Figure 3, while Figure 4 shows the differences (FR - PR) in their surface concentrations between the two simulations. In the future run, there are regions of decreases and increases in the surface concentrations of PM_f species with practically zero global average change. For most regions and species, the change in surface layer concentrations is consistent with the global trend, i.e., decrease. The factors contributing to this decrease were elaborated in the discussion on global PM_f

Table 3. Summer (June/July/August) and Winter (December/January/February) Surface Layer (984–934 hPa) Odd Oxygen (O_x) Budgets for the Eastern United States (95°–80°W, 32°–40°N)[a]

	Summer		Winter	
	PR	FR	PR	FR
Sources, Gg yr^{-1}				
Chemical production	6944	8020	953	1066
Net transport	−1208	−1707	297	232
Sinks, Gg yr^{-1}				
Chemical loss	2033	2529	410	406
Dry deposition	3703	3784	840	892
Burden, Gg	51.9	57.6	28.0	27.6
Lifetime, hours	20.0	20.2	48.4	46.0
	Summer		Winter	
Sink effect	+1.0%		−5.3%	
Source effect	+10%		+3.9%	

[a]See section 3.1.1 for the definitions of O_x and sink and source effects. The present and future runs are denoted by PR and FR.

Table 4. Annual Global Budgets for Fine PM Species[a]

	SO_4^{2-}		NO_3^-		NH_4^+		BC		POA		SOA	
	PR	FR	PR	FR	PR	FR	PR	FR	PR	FR	PR	FR
Sources, Tg yr^{-1}	28.4	28.7	28.0	26.9	20.9	21.9	12	12	81	81	16.3	14.2
Sinks, Tg yr^{-1}												
Wet deposition	24.4	24.4	23.0	22.1	16.9	17.6	7.6	7.5	49.1	49.0	12.8	11.1
Dry deposition	4.0	4.3	5.0	4.8	4.0	4.3	4.4	4.5	31.9	32.0	3.5	3.1
Burden, Tg	0.36	0.33	0.8	0.7	0.47	0.42	0.22	0.21	1.28	1.24	0.29	0.24
Lifetime, days	4.8	4.3	10.4	9.5	8.2	7.0	6.5	6.4	5.8	5.6	6.5	6.2

	SO_4^{2-}	NO_3^-	NH_4^+	BC	POA	SOA
Sink effect	−10%	−9%	−15%	−2%	−3%	−5%
Source effect	+1%	−4%	+5%	0%	0%	−13%

[a]See section 2.1.3 for the definition of fine PM. The present and future runs are denoted by PR and FR. The budget for sulfate is in TgS. See section 3.1.1 for definitions of the sink and source effects.

budgets. Here, only those regions and species that deviate significantly from the global trend are discussed in detail.

[33] The increased SO_4^{2-} concentrations over the eastern United States (100–65°W, 24–52°N) in the future run (Figure 4a) are understood better when the seasonally resolved changes in the SO_4^{2-} burden, the regional-scale precipitation, and the SO_4^{2-} produced by the gas phase and in-cloud oxidation of SO_2 are considered together. These changes are shown in Figure 5. Figure 5a shows that the SO_4^{2-} burden increased during the months May through July, and January. The SO_4^{2-} increase during the months of January, June and July (JJJ) is due to the longer SO_4^{2-} lifetime caused by reduced precipitation (Figure 5b). In this case, the SO_4^{2-} increase due to the longer lifetime outweighs the decrease caused by the reduced in-cloud SO_4^{2-} production (Figure 5d). Furthermore, the increased SO_4^{2-} production by SO_2 + OH· during the JJJ months is likely contributing to the SO_4^{2-} increase because of the longer lifetime generally associated with the SO_4^{2-} produced by the gas phase oxidation of SO_2 [*Koch et al.*, 2003]. In contrast with the SO_4^{2-} increases during the JJJ months, the increased SO_4^{2-} burden during the month of May occurs due to the increased in-cloud SO_4^{2-} production. For the remaining months, even though in-cloud SO_4^{2-} production increased significantly, the SO_4^{2-} burden decreased due to shorter lifetimes caused by increased precipitation.

[34] Analysis of the regional-scale organic PM_f budgets (not shown) suggests that the predicted increases in the annual average surface layer concentrations of POA over eastern Europe and Mediterranean (Figure 4e) as well as the increases in organic PM_f concentrations over northern Africa (Figures 4d–4f) correlate strongly with the predicted seasonal-scale precipitation decreases over these regions. It is evident that the predicted regional-scale precipitation changes play a key role in the changes of both inorganic and organic PM_f species. However, given the low statistical significance of the predicted regional-scale precipitation

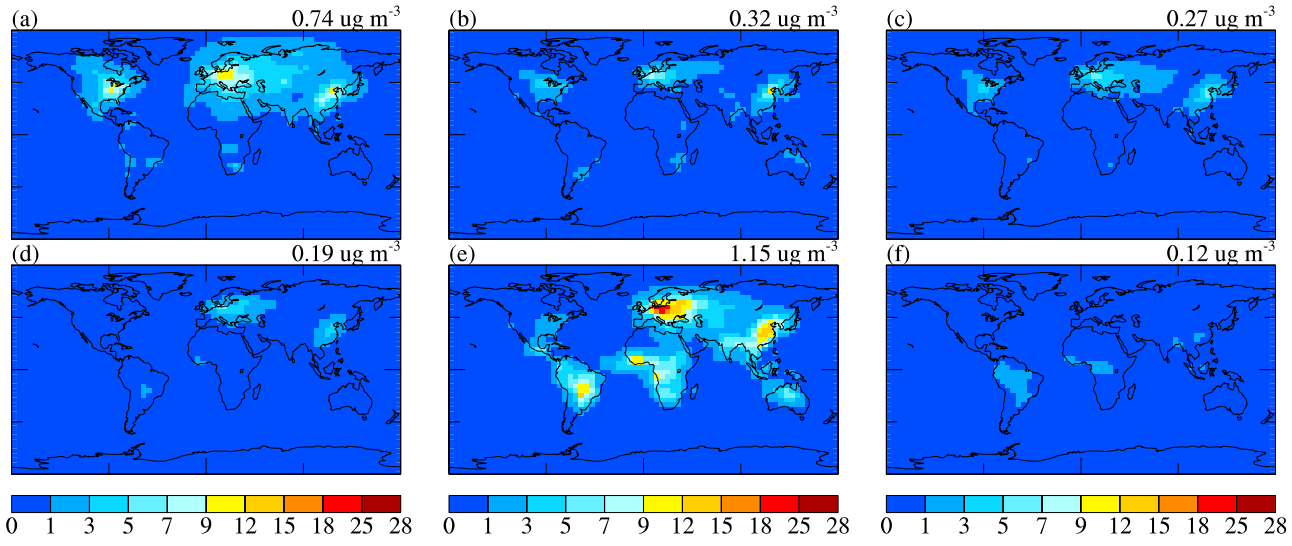

Figure 3. Surface layer (984–934 hPa) annual average concentrations (μg m^{-3}) of (a) sulfate, (b) nitrate, (c) ammonium, (d) black carbon, (e) primary organic aerosol, and (f) secondary organic aerosol in the present run. The global annual average concentrations and units are indicated above the top right corner. In each case, uniform temperature and pressure values of 298 K and 1000 hPa were used to convert aerosol mass to aerosol concentrations.

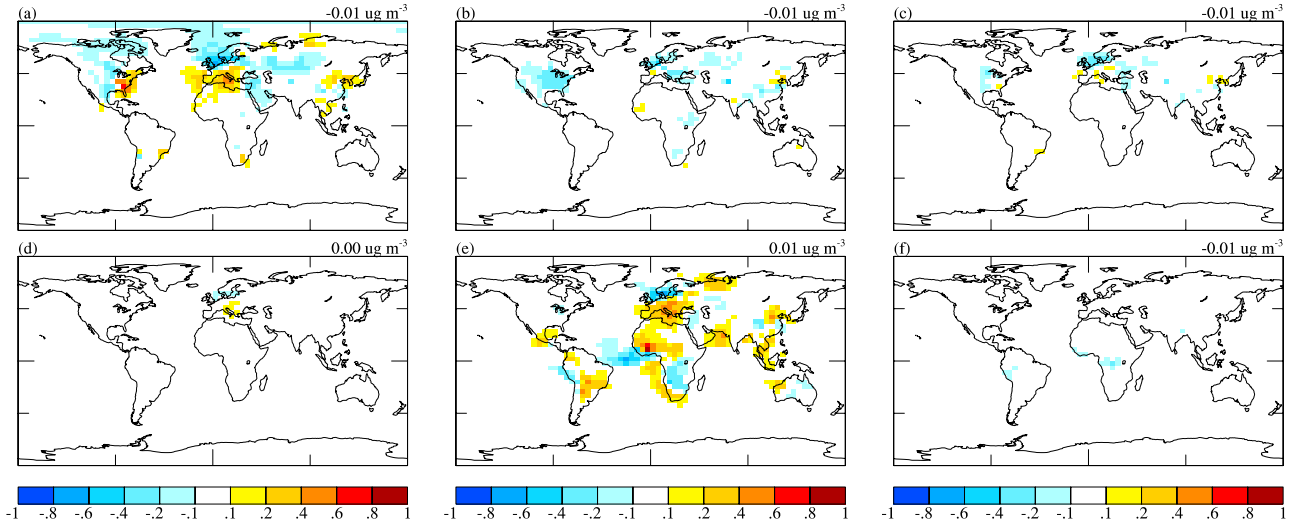

Figure 4. Surface layer (984–934 hPa) annual average differences (future run (FR) minus present run (PR)) in the concentrations (μg m^{-3}) of (a) sulfate, (b) nitrate, (c) ammonium, (d) black carbon, (e) primary organic aerosol, and (f) secondary organic aerosol. The global annual average differences and units are indicated above the top right corner. In each case, uniform temperature and pressure values of 298 K and 1000 hPa were used to convert aerosol mass to aerosol concentrations.

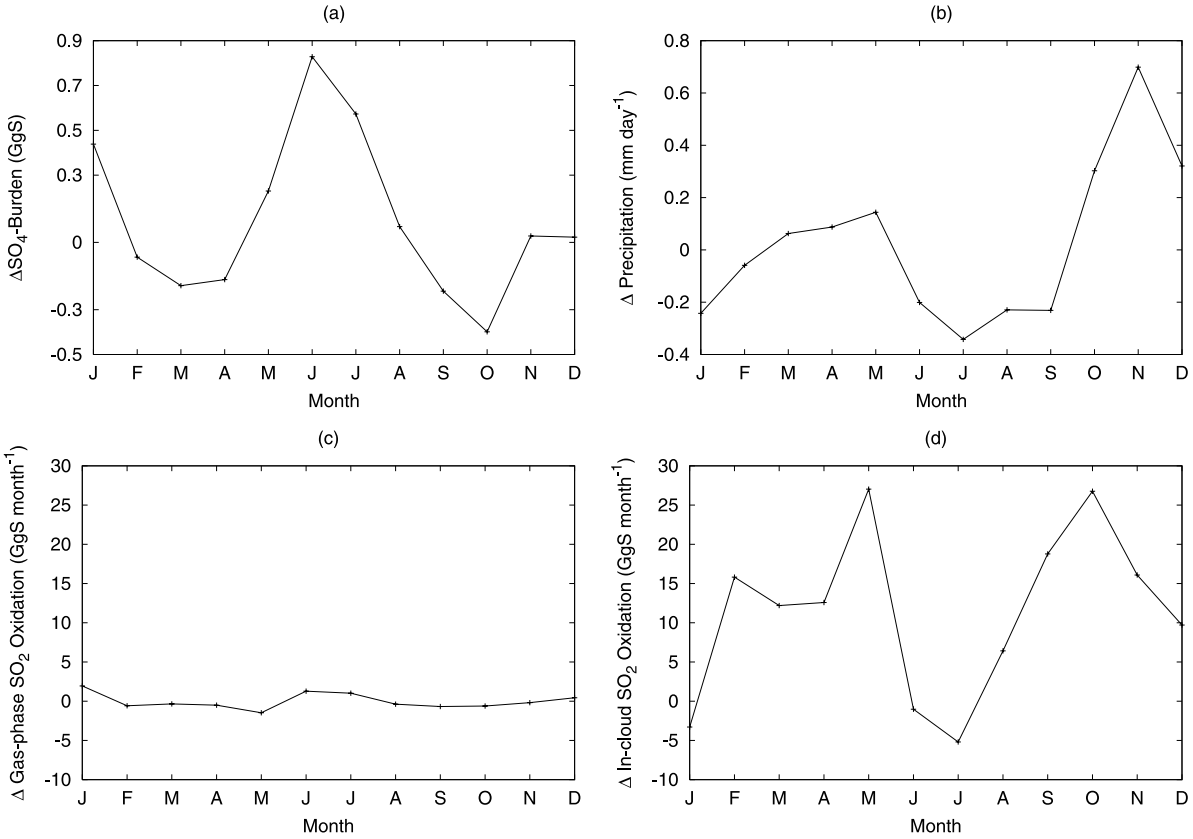

Figure 5. Monthly variation of differences (future run minus present run) in (a) SO_4^{2-} burden (GgS) in the surface layer (984–934 hPa), (b) column-integrated precipitation (mm d^{-1}), and SO_4^{2-} produced (GgS month^{-1}) by (c) gas phase and (d) aqueous phase oxidation of SO_2 in the surface layer (984–934 hPa) of the eastern United States. Months J through D refer to the months January through December, and each month represents a 5-year average for that month.

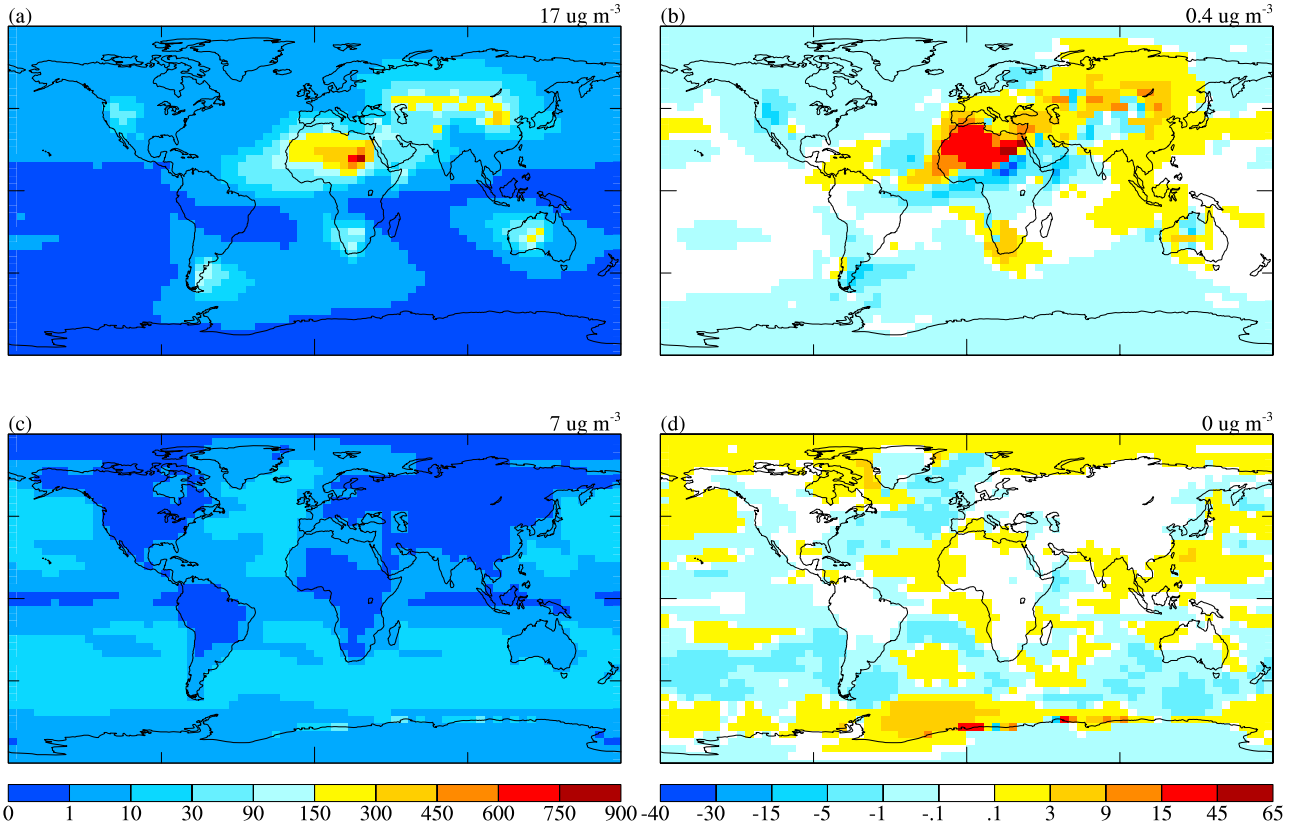

Figure 6. Surface layer (984–934 hPa) annual average concentrations (μg m^{-3}) and differences (future run (FR) minus present run (PR)) in concentrations of (a and b) dust and (c and d) sea salt. The global annual average concentrations (or differences) and units are indicated above the top right corner. In each case, uniform temperature and pressure values of 298 K and 1000 hPa were used to convert aerosol mass to aerosol concentrations.

changes, the regional-scale fine particulate matter changes have a significant uncertainty (see section 2.3).

3.3. Dust and Sea Salt

[35] Annual average surface layer concentrations of dust and sea salt in the present run are shown in Figures 6a and 6c, while Figures 6b and 6d show the differences (FR − PR) in their surface layer concentrations between the two simulations. As expected, the highest present-day concentrations of dust are found over the Sahara and Gobi deserts, while the highest sea salt concentrations are found over the Southern Ocean. In the future run, large increases in the surface layer concentrations of dust are predicted over the Sahara and Gobi deserts. When compared to the changes in dust concentrations, the changes in sea salt concentrations are relatively small. The dust budgets for these regions (not shown) suggests that this increase is primarily due to reduced wet deposition associated with decreased regional-scale precipitation. On a seasonal scale, increased dust emissions associated with the increased wind speeds also play a minor role. As can be seen from Figure 6b, the model results suggest that increases in dust emissions over source regions such as the Sahara desert could increase the dust concentrations over nearby regions. However, given the large uncertainties associated with total dust emissions as well as their size distribution, it is difficult to predict implications for fine PM.

4. Summary and Conclusions

[36] The sensitivity of ozone and fine particulate matter concentrations to climate change is demonstrated by performing simulations corresponding to present and future climates using an integrated model of global climate, tropospheric gas phase chemistry and aerosols. Future climate is imposed using ocean boundary conditions corresponding to the IPCC SRES A2 scenario for the 2050s decade, resulting in an increase in the global annual average values of the surface air temperature by 1.7°C, the lower tropospheric specific humidity by 0.9 g H_2O/kg air, and the precipitation by 0.15 mm d^{-1}. Present-day anthropogenic emissions were used in both simulations while climate-sensitive natural emissions were allowed to vary with the simulated climate.

[37] The future simulation shows that the tropospheric ozone burden and lifetime decrease significantly in a warmer climate. For example, it was found that the tropospheric ozone burden decreased by 17 Tg (5.6%) and the tropospheric ozone lifetime decreased from 27.8 to 25.3 days. These decreases are primarily driven by increased ozone loss rates through ozone photolysis in the presence of

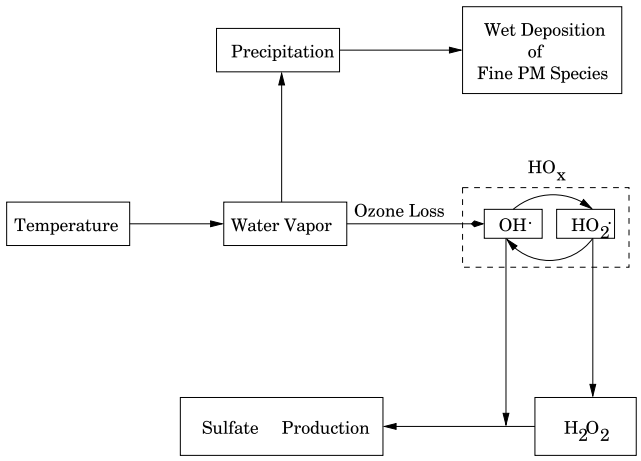

Figure 7. Central role of water and water vapor in the predicted changes for ozone and fine particulate matter species in the future climate simulation.

water vapor, which in turn is a result of increased water vapor concentrations associated with higher temperatures. On a global scale, the ozone chemical production increased by 145 Tg yr^{-1} (3.6%) in the future simulation. This increase is more than countered by increased ozone loss rates.

[38] At the surface layer, over most remote regions (marine or unpolluted), the annual average ozone mixing ratios decreased by 1–3 ppbv. In contrast, regions with high ozone precursor emissions showed relatively smaller decreases of 0–1 ppbv and increases of 1–5 ppbv over regions such as the eastern United States. These changes display a strong seasonality in ozone chemical production and ozone loss. For example, over the eastern United States, it was found that the increased annual average ozone mixing ratios were driven by summertime increases that resulted from increased ozone chemical production, and to some extent due to slower dry deposition.

[39] In the future simulation, the global burdens and the lifetimes of all the fine particulate matter species decreased 2–18% relative to the present simulation, due to the increased wet deposition removal rates associated with the increased global annual average precipitation. While precipitation effects dominate the response of other species, the decreased burden of secondary organic aerosol is primarily due to reduced partitioning of gas phase secondary organics into the aerosol phase, as a result of warmer temperatures.

[40] At the surface layer, the future simulation shows that there are regions of decreases and increases in the concentrations of fine particulate matter species with practically zero global annual average change. The monthly surface layer budgets for the fine particulate matter species suggests that regional-scale precipitation changes are key to these changes. For example, it was found that over the eastern United States, sulfate concentrations increased by nearly 1 μg m^{-3} during the months of June and July due to the reduced precipitation during those months. However, given the low statistical significance of the predicted regional-scale precipitation changes, the regional-scale fine particulate matter changes have a significant uncertainty. Nevertheless, these results underscore the key role that precipitation changes will play with respect to fine particulate matter concentrations in future climate scenarios.

[41] Collectively, these simulations demonstrate that changes in the hydrologic cycle in future climate scenarios, will play a key role in the changes of both ozone and fine particulate matter concentrations. The central role of water and water vapor with respect to the predicted changes in this study is summarized in Figure 7. With regards to the robustness of the predicted changes in the hydrologic cycle, regional-scale changes in precipitation and liquid water content are highly uncertain. A better representation of cloud and related processes in further work will help reduce this uncertainty. However, the increased water vapor levels and global precipitation predicted in the current study are consistent with the predictions of other climate models in a warmer climate scenario [*Soden et al.*, 2005; *Allen and Ingram*, 2002; *IPCC*, 2001]. Hence model predictions such as the decreased global burdens of ozone and fine particulate matter species are robust.

[42] **Acknowledgments.** This work was supported by the National Center for Environmental Research (NCER) STAR Program, EPA (agreement RD-83096101-0). The authors thank two anonymous reviewers for their insightful suggestions. We also thank Hong Liao at Caltech and Loretta Mickley at Harvard University for the support they provided with the "unified" model. Finally, we thank Rick Healy at Woods Hole Oceanographic Institute for providing the future ocean boundary conditions used in this work and generous support with the GISS GCM II′ model.

References

Adams, P. J., J. H. Seinfeld, and D. M. Koch (1999), Global concentrations of tropospheric sulfate, nitrate, and ammonium aerosol simulated in a general circulation model, *J. Geophys. Res.*, *104*(D11), 13,791–13,823.

Allen, M. R., and W. J. Ingram (2002), Constraints on future changes in climate and the hydrologic cycle, *Nature*, *419*, 224–232.

Appenzeller, C., J. R. Holton, and K. H. Rosenlof (1996), Seasonal variation of mass transport across the tropopause, *J. Geophys. Res.*, *101*(D10), 15,071–15,078.

Aw, J., and M. J. Kleeman (2003), Evaluating the first-order effect of intra-annual temperature variability on urban air pollution, *J. Geophys. Res.*, *108*(D12), 4365, doi:10.1029/2002JD002688.

Baertsch-Ritter, N., J. Keller, J. Dommen, and A. S. H. Prevot (2004), Effects of various meteorological conditions and spatial emission resolutions on the ozone concentration and ROG/NOx limitation in the Milan area (I), *Atmos. Chem. Phys.*, *4*, 423–438.

Bauer, S. E., and D. Koch (2005), Impact of heterogeneous sulfate formation at mineral dust surfaces on aerosol loads and radiative forcing in the Goddard Institute for Space Studies general circulation model, *J. Geophys. Res.*, *110*, D17202, doi:10.1029/2005JD005870.

Bian, H. S., and C. S. Zender (2003), Mineral dust and global tropospheric chemistry: Relative roles of photolysis and heterogeneous uptake, *J. Geophys. Res.*, *108*(D21), 4672, doi:10.1029/2002JD003143.

Cess, R. D., et al. (1990), Intercomparison and interpretation of climate feedback processes in 19 atmospheric general-circulation models, *J. Geophys. Res.*, *95*(D10), 16,601–16,615.

Chung, S. H., and J. H. Seinfeld (2002), Global distribution and climate forcing of carbonaceous aerosols, *J. Geophys. Res.*, *107*(D19), 4407, doi:10.1029/2001JD001397.

Collins, W. J., R. G. Derwent, B. Garnier, C. E. Johnson, M. G. Sanderson, and D. S. Stevenson (2003), Effect of stratosphere-troposphere exchange on the future tropospheric ozone trend, *J. Geophys. Res.*, *108*(D12), 8528, doi:10.1029/2002JD002617.

Del Genio, A. D., and M. S. Yao (1993), Efficient cumulus parameterization for long-term climate studies: The GISS scheme, *Meteorol. Monogr.*, *46*, 181–184.

Del Genio, A. D., M. S. Yao, W. Kovari, and K. K. W. Lo (1996), A prognostic cloud water parameterization for global climate models, *J. Clim.*, *9*(2), 270–304.

Dockery, D. W., C. A. Pope, X. P. Xu, J. D. Spengler, J. H. Ware, M. E. Fay, B. G. Ferris, and F. Speizer (1993), An association between air-pollution and mortality in 6 United States cities, *New England J. Med.*, *329*(24), 1753–1759.

Guenther, A., et al. (1995), A global-model of natural volatile organic-compound emissions, *J. Geophys. Res.*, *100*(D5), 8873–8892.

Hallquist, M., D. J. Stewart, S. K. Stephenson, and R. A. Cox (2003), Hydrolysis of N_2O_5 on sub-micron sulfate aerosols, *Phys. Chem. Chem. Phys.*, *5*(16), 3453–3463.

Hansen, J., G. Russell, D. Rind, P. Stone, A. Lacis, S. Lebedeff, R. Ruedy, and L. Travis (1983), Efficient 3-dimensional global-models for climate studies: MODEL-I and MODEL-II, *Mon. Weather Rev.*, *111*(4), 609–662.

Intergovernmental Panel on Climate Change (IPCC) (2001), *Climate Change 2001: The Scientific Basis*, Cambridge Univ. Press, New York.

Johnson, C. E., D. S. Stevenson, W. J. Collins, and R. G. Derwent (2001), Role of climate feedback on methane and ozone studied with a coupled ocean-atmosphere-chemistry model, *Geophys. Res. Lett.*, *28*(9), 1723–1726.

Kane, S. M., F. Caloz, and M. T. Leu (2001), Heterogeneous uptake of gaseous N_2O_5 by $(NH_4)_2SO_4$, NH_4HSO_4, and H_2SO_4 aerosols, *J. Phys. Chem. A*, *105*(26), 6465–6470.

Kettle, A. J., et al. (1999), A global database of sea surface dimethylsulfide (DMS) measurements and a procedure to predict sea surface DMS as a function of latitude, longitude, and month, *Global Biogeochem. Cycles*, *13*(2), 399–444.

Koch, D. (2001), Transport and direct radiative forcing of carbonaceous and sulfate aerosols in the GISS GCM, *J. Geophys. Res.*, *106*(D17), 20,311–20,332.

Koch, D., D. Jacob, I. Tegen, D. Rind, and M. Chin (1999), Tropospheric sulfur simulation and sulfate direct radiative forcing in the Goddard Institute for Space Studies general circulation model, *J. Geophys. Res.*, *104*(D19), 23,799–23,822.

Koch, D., J. Park, and A. Del Genio (2003), Clouds and sulfate are anticorrelated: A new diagnostic for global sulfur models, *J. Geophys. Res.*, *108*(D24), 4781, doi:10.1029/2003JD003621.

Krewski, D., R. T. Burnett, M. S. Goldberg, B. K. Hoover, J. Siemiatycki, M. Jerrett, M. Abrahamowicz, and W. H. White (2003), Overview of the reanalysis of the Harvard Six Cities Study and American Cancer Society Study of particulate air pollution and mortality, *J. Toxicol. Environ. Health, Part A*, *66*(16–19), 1507–1551.

Levitus, S. (1982), Climatological atlas of the world ocean, *NOAA Prof. Pap. 13*, 173 pp., NOAA, Silver Spring, Md.

Liao, H., P. J. Adams, S. H. Chung, J. H. Seinfeld, L. J. Mickley, and D. J. Jacob (2003), Interactions between tropospheric chemistry and aerosols in a unifiegeneral circulation model, *J. Geophys. Res.*, *108*(D1), 4001, doi:10.1029/2001JD001260.

Liao, H., J. H. Seinfeld, P. J. Adams, and L. J. Mickley (2004), Global radiative forcing of coupled tropospheric ozone and aerosols in a unified general circulation model, *J. Geophys. Res.*, *109*, D16207, doi:10.1029/2003JD004456.

Liao, H., W.-T. Chen, and J. H. Seinfeld (2006), Role of climate change in global predictions of future tropospheric ozone and aerosols, *J. Geophys. Res.*, *111*, D12304, doi:10.1029/2005JD006852.

Logan, J. A. (1999), An analysis of ozonesonde data for the lower stratosphere: Recommendations for testing models, *J. Geophys. Res.*, *104*(D13), 16,151–16,170.

Mickley, L. J., P. P. Murti, D. J. Jacob, J. A. Logan, D. M. Koch, and D. Rind (1999), Radiative forcing from tropospheric ozone calculated with a unified chemistry-climate model, *J. Geophys. Res.*, *104*(D23), 30,153–30,172.

Rind, D., and J. Lerner (1996), Use of on-line tracers as a diagnostic tool in general circulation model development: 1. Horizontal and vertical transport in the troposphere, *J. Geophys. Res.*, *101*(D7), 12,667–12,683.

Rind, D., J. Lerner, K. Shah, and R. Suozzo (1999), Use of on-line tracers as a diagnostic tool in general circulation model development: 2. Transport between the troposphere and stratosphere, *J. Geophys. Res.*, *104*(D8), 9151–9167.

Robertson, A., et al. (2001), Hypothesized climate forcing time series for the last 500 years, *J. Geophys. Res.*, *106*(D14), 14,783–14,803.

Russell, G. L., J. R. Miller, and D. Rind (1995), A coupled atmosphere-ocean model for transient climate change studies, *Atmos. Ocean*, *33*(4), 683–730.

Schwartz, J. (1996), Air pollution and hospital admissions for respiratory disease, *Epidemiology*, *7*(1), 20–28.

Sillman, S., and F. J. Samson (1995), Impact of temperature on oxidant photochemistry in urban, polluted rural and remote environments, *J. Geophys. Res.*, *100*(D6), 11,497–11,508.

Soden, B. J., D. L. Jackson, V. Ramaswamy, M. D. Schwarzkopf, and X. L. Huang (2005), The radiative signature of upper tropospheric moistening, *Science*, *310*, 841–844.

Stevenson, D. S., C. E. Johnson, W. J. Collins, R. G. Derwent, and J. M. Edwards (2000), Future estimates of tropospheric ozone radiative forcing and methane turnover: The impact of climate change, *Geophys. Res. Lett.*, *27*(14), 2073–2076.

Thornton, J. A., C. F. Braban, and J. P. D. Abbatt (2003), N_2O_5 hydrolysis on sub-micron organic aerosols: The effect of relative humidity, particle phase, and particle size, *Phys. Chem. Chem. Phys.*, *5*(20), 4593–4603.

Wang, Y. H., D. J. Jacob, and J. A. Logan (1998), Global simulation of tropospheric O_3-NO_x-hydrocarbon chemistry: 1. Model formulation, *J. Geophys. Res*, *103*(D9), 10,713–10,725.

Wesely, M. L. (1989), Parameterization of surface resistances to gaseous dry deposition in regional-scale numerical-models, *Atmos. Environ.*, *23*(6), 1293–1304.

P. J. Adams, Department of Civil and Environmental Engineering, Carnegie Mellon University, Porter Hall 113, Pittsburgh, PA 15213, USA. (peteradams@cmu.edu)

P. N. Racherla, Department of Engineering and Public Policy, Carnegie Mellon University, Baker Hall 128-C, Pittsburgh, PA 15213, USA. (pavanracherla@cmu.edu)